Virus Research 343 (2024) 199356

Contents lists available at ScienceDirect

Virus Research

journal homepage: www.elsevier.com/locate/virusres

Drug repurposing screen to identify inhibitors of the RNA polymerase (nsp12) and helicase (nsp13) from SARS-CoV-2 replication and transcription complex

Maria Kuzikov [a,b,*], Jeanette Reinshagen [a], Krzysztof Wycisk [c], Angela Corona [d], Francesca Esposito [d], Paolo Malune [d], Candida Manelfi [e], Daniela Iaconis [e], Andrea Beccari [e], Enzo Tramontano [d], Marcin Nowotny [c], Björn Windshügel [a,b], Philip Gribbon [a], Andrea Zaliani [a]

[a] Fraunhofer Institute for Translational Medicine and Pharmacology (ITMP) and Fraunhofer Cluster of Excellence for Immune mediated diseases (CIMD), Schnackenburgallee 114, 22525 Hamburg, and Theodor Stern Kai 7, 60590 Frankfurt, Germany
[b] Constructor University, School of Science, Campus Ring 1, 28759 Bremen, Germany
[c] Laboratory of Protein Structure - International Institute of Molecular and Cell Biology, 4 Ks. Trojdena Street, 02-109 Warsaw, Poland
[d] Dipartimento di Scienze della vita e dell'ambiente, Cittadella Universitaria di Monserrato, SS-554, Monserrato, Cagliari, Italy
[e] EXSCALATE, Dompé farmaceutici S.p.A., Via Tommaso De Amicis, 95, Napoli, 80131, Italy

ARTICLE INFO

Keywords:
SARS-CoV-2
Helicase
RNA-dependent RNA polymerase
Screening
Drug repurposing

ABSTRACT

Coronaviruses contain one of the largest genomes among the RNA viruses, coding for 14–16 non-structural proteins (nsp) that are involved in proteolytic processing, genome replication and transcription, and four structural proteins that build the core of the mature virion. Due to conservation across coronaviruses, nsps form a group of promising drug targets as their inhibition directly affects viral replication and, therefore, progression of infection. A minimal but fully functional replication and transcription complex was shown to be formed by one RNA-dependent RNA polymerase (nsp12), one nsp7, two nsp8 accessory subunits, and two helicase (nsp13) enzymes. Our approach involved, targeting nsp12 and nsp13 to allow multiple starting point to interfere with virus infection progression. Here we report a combined in-vitro repurposing screening approach, identifying new and confirming reported SARS-CoV-2 nsp12 and nsp13 inhibitors.

1. Introduction

Since its identification in December 2019, increasing numbers of accumulated viral mutations have been reported for SARS-CoV-2 which developed to variants of concerns (VOC) such as Omicron, B.1.1.529 (WHO, 2023; Covariants, 2023). Such variants exhibit immune escape and/or diverse disease progression. This development raises challenges, both in terms of long-term effectiveness of current vaccines, but also the increases the need to focus on therapeutic interventions against SARS-CoV-2 genome targets which may be less predisposed to mutagenesis. Phylogenetic analysis of human coronaviruses (HCoV) and the bat coronavirus RaTG13, a close relative of SARS-CoV-2, showed a high degree of conservation within the helicase (nsp13) region, revealing it as a promising conserved protein target suitable for drug development (Spratt et al., 2021). At the outset of the SARS-CoV-2 pandemic, RNA-dependent RNA polymerase (RdRp, nsp12) was determined as a promising antiviral target, since the enzyme plays a key role in replication of viral genome and progression of infection, as well as having no close host-cell homologs, a potential benefit in terms of reduced off-target effects. Therefore, targeting both nsp13 and nsp12, either by a single treatment or with a combination therapy, provides an emergingapproach to modulate COVID-19 infection.

1.1. Structure and function of SARS-CoV-2 minimal replication and transcription complex

Coronavirus replication machinery involves an interplay of non-structural proteins (nsp): nsp7, nsp8, nsp9, nsp10, nsp11, nsp12, nsp13, nsp14, nsp15 and nsp16, regulating replication and transcription, unwinding, proofreading and RNA capping functions (Malone

* Corresponding author at: Fraunhofer Institute for Translational Medicine and Pharmacology (ITMP) and Fraunhofer Cluster of Excellence for Immune mediated diseases (CIMD), Schnackenburgallee 114, 22525 Hamburg, and Theodor Stern Kai 7, 60590 Frankfurt, Germany.
E-mail address: maria.kuzikov@itmp.fraunhofer.de (M. Kuzikov).

https://doi.org/10.1016/j.virusres.2024.199356
Received 28 August 2023; Received in revised form 26 February 2024; Accepted 13 March 2024
Available online 16 March 2024

et al., 2022). A minimal, but fully functional replication and transcription complex was shown to be formed by one nsp12, one nsp7/nsp8 heterodimer, a nsp8 accessory subunit, along with two nsp13 bound to one template RNA strand (Yan et al., 2020; Peng et al., 2020; Kirchdoerfer and Ward, 2019). Nsp12 was shown to form the typical polymerase cupped right-hand structure (Peng et al., 2020; Kirchdoerfer and Ward, 2019). The active site is located in the palm domain, with the loop of the finger domain bridging over it to reach the thumb domain, leading to a comparatively closed channel, in contrast to the more open form of RdRp observed with negative strand RNA viruses (Peng et al., 2020; Kirchdoerfer and Ward, 2019; Gorbalenya et al., 2002). The fingers-thumb interaction region also contains the binding site for the nsp7-nsp8 heterodimer (Kirchdoerfer and Ward, 2019). Nsp7 and nsp8 were shown to stimulate the activity of nsp12, through stabilisation of nsp12 regions involved in RNA binding (Peng et al., 2020; Ahn et al., 2012; Subissi et al., 2014). The polymerisation activity of SARS-CoV nsp12 was shown to be Mg^{2+}- and Mn^{2+}-dependent, whereby the initiation of polymerisation occurs both primer-depended and as *de novo* synthesis, in contrast to human polymerase (Kirchdoerfer and Ward, 2019; te Velthuis et al., 2010). For SARS-CoV and MERS viruses it was shown that nsp12 can enhance the unwinding and ATPase activities of nsp13 (Jia et al., 2019). Nsp13 is essential for the viral replication, it is hypothesized that the ability of nsp13 to open the duplex in 5′ to 3′ direction is used to release the -ssRNA strand associated with the free 3′ end, from the RNA-duplex during replication (Tanner et al., 2003). Nsp13 is a multi-domain protein with NTPase/helicase activity in SARS-CoV-2. The N-terminal domain contains a zinc-binding domain with twelve conserved cysteine and histidine residues that form a binuclear Zn^{2+}-binding pocket that is essential for the helicase activity (Ulferts et al., 2010). The C-terminal domains harbours the enzymatic activity (Ulferts et al., 2010; Jia et al., 2019). Characterisation of the enzymatic activity of SARS-CoV-2 as well as SARS-CoV nsp13 revealed that the enzyme unwinds both double-stranded DNA and RNA in a 5′−3′direction. If a 5′ single strand is present (Tanner et al., 2003; Ivanov et al., 2004; Sommers et al., 2023). Nsp13 of SARS-CoV-2 is capable of hydrolysing all deoxyribonucleotide (dNTPs) and ribonucleotide triphosphates (NTPs) in presence of Mg^{2+} (Tanner et al., 2003).

1.2. Known inhibitors of coronavirus RdRp with reported anti-viral activity

The first drug approved for treatment of severe COVID-19 infections was Veklury (remdesivir) (FDA, 2021; EMA, 2021), and, like the majority of known RdRp inhibitors, it is a nucleotide-base analogue. The pro-drug, Remdesivir is a monophosphoramidate adenosine analogue with broad inhibitory activity against multiple virus families among them *Filoviridae, Coronaviridae* and *Orthomyxoviridae* (Eastman et al., 2020; Gordon et al., 2020). The Remdesivir metabolite competes with adenosine triphosphate (ATP), inhibiting RdRp function through delayed termination of transcription (Eastman et al., 2020; Gordon et al., 2020). Other nucleotide-base analogue RdRp inhibitors are favipiravir (Avigan) and molnupiravir (Joshi et al., 2021; Yoon et al., 2018). Favipiravir is acting as a mutagenic nucleoside and chain terminator (Joshi et al., 2021). Molnupiravir is a nucleoside analogue, originally proposed for inhibition of influenza and respiratory syncytial virus (Yoon et al., 2018). It is recognized by the RdRp as a cytidine or uridine triphosphates resulting in C-U and G-A transitions and thus increasing the mutation rate (Sheahan et al., 2020). Suramin is a non-nucleoside, non-prodrug inhibitor which was reported to inhibit SARS-CoV-2 RdRp *in-vitro*. This compound showed a 20-fold stronger inhibition of SARS-CoV-2 RdRp compared to Remdesivir in a biochemical readout (Yin et al., 2021). The activity of suramin was confirmed in cell-based virus replication assays, and its binding to the RdRp complex of nsp12, nsp7 and nsp8 demonstrated in cryo-EM (Yin et al., 2021). The compound, SSYA10-001, is a well characterized SARS-CoV helicase inhibitors which acts non-competitively with respect to the ATP and the nucleic acid substrate, and has antiviral activity against SARS, MERS-CoV in infected VeroE6 cells (Adedeji et al., 2012, 2014). Flavonoids, including myricetin and scutellarin were shown to inhibit helicase of SARS-CoV reducing its ATPase activity in vitro (but not the unwinding function) (Yu et al., 2012). Recently, we confirmed the activity of natural flavonoids against SARS-CoV-2 helicase (Corona et al., 2022). Suramin is a potent inhibitor in a FRET-based helicase assays as well as in a cellular model for SARS-CoV-2 infection (Zeng et al., 2021). However, the observed cytopathic effect might be due to suramin related inhibition of RdRp (Yin et al., 2021).

Taking into account the reported structural specificities of nsp12 and nsp13, we have developed a screening pipeline to test a large collection of drug-like and repurposed molecules in order to identify starting points for the development of effective antiviral drugs with potential dual activity against both targets.

2. Material and methods

The drug repurposing approach to find novel inhibitors for a minimal replication complex was started using a nsp12/7/8 complex with nsp12 and nsp7/8 separately expressed and purified. In the first period of the studies, nsp8 sequence of SARS-CoV was cloned in the construct, in place of SARS-CoV-2, resulting in a difference of five amino acids (F3957Y; I4074V; N4078G; T4087N; S4115N) (Suppl. Fig. 1). All other nsps were used from SARS-CoV-2. The amino acids are located at the outer side of nsp8, distant from to the interaction areas with nsp12 (Suppl. Fig. 2). Substitutions in the amino acids of nsp8 between SARS-CoV-2 and SARS-CoV were recently reported to result in lower melting temperature (Tm) values, suggesting limited thermostability of SARS-CoV-2 nsp8 (Peng et al., 2020). The sequence exchange of nsp8 was identified after the end of the screening campaign. Which led to reconfirmation of enzymatic activity, assay performance and re-validation of identified hits using the corrected nsp12/7/8 complex (Suppl. Figs. 3 and 4). No significant difference in enzymatic activity or inhibition potency was observed towards both used constructs.

2.1. Protein expression and purification

2.1.1. nsp13—used for primary screening and hit profiling

Nsp13 was expressed from pNIC-ZB vector (Addgene #159614; GenBank ID: NC_045512.2) in Rosetta cells in TB medium. Protein was purified according to literature (Newman et al., 2021). Briefly, bacterial cells were suspended in buffer A (50 mM HEPES, pH 7.5; 500 mM NaCl; 5 % glycerol; 10 mM imidazole; 0.5 mM TCEP) with addition of proteases inhibitors. After sonication and centrifugation supernatant was loaded onto HisTrap HP column equilibrated with buffer A. The column was washed sequentially with buffer containing 45 mM imidazole, 1 M NaCl and again 45 mM imidazole. Protein was eluted with buffer B (50 mM HEPES, pH 7.5; 500 mM NaCl; 5 % glycerol; 300 mM imidazole; 0.5 mM TCEP). Eluted fractions were immediately loaded onto HiTrap SP column and nsp13 eluted with Hi-salt buffer (50 mM HEPES, pH 7.5; 1000 mM NaCl; 5 % glycerol; 0.5 mM TCEP). After overnight digestion with TEV protease, nsp13 was further purified using HiLoad Superdex 200 pg column equilibrated with SEC buffer (50 mM HEPES, pH 7.5; 500 mM NaCl; 0.5 mM TCEP). The final yield was 4 mg of protein from a 4 l culture.

2.1.2. nsp12—used for primary screening and hit profiling

Nsp12 (GenBank: WGR02155.1) was expressed from pET-28a (+) vector in BL21-Gold (DE3) cells in LB medium. Bacterial cells were suspended in buffer A (20 mM Tris–HCl, pH 8.0; 500 mM NaCl; 4 mM $MgCl_2$; 1 mM DTT; 5 % glycerol; 10 mM imidazole) with addition of proteases inhibitors. After sonication and centrifugation supernatant was loaded onto a HisTrap HP column equilibrated with buffer A. The column was washed with buffer containing 100 mM imidazole and protein eluted with buffer B (20 mM Tris–HCl; pH 8.0; 500 mM NaCl; 4

mM $MgCl_2$; 1 mM DTT; 5 % glycerol; 300 mM imidazole). After overnight digestion with SUMO protease protein was loaded onto HisTrap HP column and nsp12 present in flow through was collected and concentrated. Protein was further purified using HiLoad Superdex 200 pg column equilibrated with SEC buffer (50 mM HEPES, pH 7.0; 100 mM NaCl; 4 mM $MgCl_2$). The final yield was 3 mg of protein from 4 l culture.

2.1.3. nsp7/8—used for primary screening and hit profiling

Nsp7/8 (nsp7 GenBank: UKA89184.1, nsp8 GenBank: AEA10621.1) complex was expressed from pET-21a (+) vector (nsp7) and pET-28-SUMO vector (nsp8) in BL21-Gold (DE3) cells in LB medium. Bacterial cells were suspended in buffer A (20 mM Tris–HCl, pH 7.5; 250 mM NaCl; 4 mM $MgCl_2$; 5 mM β-MeOH; 5 % glycerol; 20 mM imidazole) with addition of proteases inhibitors. After sonication and centrifugation, SUMO protease was added and the supernatant incubated for 2 h in 4 °C. Subsequently, supernatant was loaded onto HisTrap HP column equilibrated with buffer A. Column was washed with buffer containing 100 mM imidazole and proteins were eluted with buffer B (20 mM Tris–HCl; pH 7.5; 250 mM NaCl; 4 mM $MgCl_2$; 5 mM β-MeOH; 5 % glycerol; 300 mM imidazole). After overnight digestion with TEV protease proteins were loaded onto HisTrap HP column and nsp7/8 complex present in flow through was collected and concentrated. Proteins were further purified using HiLoad Superdex 200 pg column equilibrated with SEC buffer (50 mM HEPES, pH 7.0; 100 mM NaCl; 4 mM $MgCl_2$). The final yield was 12 mg of complex from 4 l culture.

2.1.4. nsp12/7/8 complex—used for revalidation in hit profiling

Nsp12/7/8 complex was expressed from pRSFDuet-1(nsp8-nsp7) (nsp12) vector (Addgene #165451; GenBank ID: nsp12 QIZ64668.1, nsp8 QIZ64668.1, nsp7 QIZ64668.1) in BL21(DE3) Star cells in LB medium. Proteins were purified according to published protocols. (Madru et al., 2021). Briefly, bacterial cells were suspended in buffer A (50 mM Tris–HCl, pH 8.0; 500 mM NaCl; 10 mM imidazole) with addition of proteases inhibitors. After sonication and centrifugation supernatant was loaded onto HisTrap HP column equilibrated with buffer A. Proteins were eluted with linear gradient of buffer B (50 mM Tris–HCl, pH 8.0; 500 mM NaCl; 500 mM imidazole). Eluted fractions were diluted 10 times with 50 mM Tris–HCl, pH 8.0) and loaded onto HiTrap Q column equilibrated with buffer C (50 mM Tris–HCl, pH 8.0; 150 mM NaCl). Proteins were eluted with linear gradient of NaCl. After overnight digestion with TEV protease proteins were concentrated and further purified using HiLoad Superdex 200 pg column equilibrated with SEC buffer (20 mM Tris–HCl, pH 8.0; 300 mM NaCl; 1 mM $MgCl_2$). The final yield was 5 mg of complex from 4 l culture.

2.2. RdRp fluorescence assay

Test compounds, as positive (20 μM suramin) and negative (100 % DMSO) controls, were transferred to 384-well assay microplates (Corning® Low Volume 384-well Black Flat Bottom Polystyrene NBS Microplate, Prod. Nr 3820) by acoustic dispensing (Echo 550R, Labcyte Inc., San José, CA, USA). Nsp12-nsp7-nsp8 were preincubated on ice for 15 min to form a complex. 2.5 μL of nsp12-nsp7-nsp8 complex diluted in assay buffer (Tris–HCl 50 mM pH 8, NaCl 50 mM, MgCl2 2.5 mM, 2 mM DTT) were added to wells. Enzyme was preincubated with compounds for 20 min at RT before addition of 2.5 μL ATP/oligo U-template mix and 2.5 μL Quant-iT™ PicoGreen™ (ThermoFisher, #P7589). Final concentrations were: compounds 20 μM, suramin 20 μM, 0.2 v/V % DMSO, 300 nM nsp12 and 900 nM nsp7/8, 100 μM ATP, 2.5 μM oligo U template and 1x Quant-iT™ PicoGreen™. Plates were sealed with aluminium foil during incubation time. Fluorescence signal was measured directly after Quant-iT™ PicoGreen™ addition, after 180 min and 24 h incubation at RT using Ex/Em of 485/535 nm (2103 EnVision™ HTS Microplate Imager, PerkinElmer, USA). The signal changes over time (FI_{t180}-FI_{t0}) were used to identify compounds inhibiting RdRp activity.

The screened compounds belong to the Fraunhofer repurposing collection, which has been assembled based on guidelines reported for the Broad repurposing collection (Broad Institute, 2023; Kuzikov et al., 2021). The Fraunhofer repurposing collection contains 5632 compounds including 3400 compounds that have reached clinical use across 600 indications, as well as 1582 preclinical compounds with varying degrees of validation (Kuzikov et al., 2021). All compounds were stored at −20 °C in 100 % DMSO prior to use.

2.3. Helicase unwinding assay

First BHQ-2- and Cy3-labelled strands were annealed for 30 min at RT by combining them in assay buffer (20 mM Tris–HCl pH7.2, 50 mM NaCl, 5 mM $MgCl_2$) containing 0.01 % Tween20 and 2 mM ATP. By the end of incubation time capture strand was added. The screen was performed in 384-well assay microplates (Corning® Low Volume 384-well Black Flat Bottom Polystyrene NBS Microplate, Prod. Nr 3820). 20 nL/well of test compounds, positive (suramin) and negative (0.2 % DMSO) controls, were transferred by acoustic dispensing (Echo 550R, Labcyte Inc., San José, CA, USA). SARS-CoV-2 helicase was diluted in assay buffer, added to wells and incubated with compounds and controls for 20 min at RT. By the end of incubation time the annealed dsDNA substrate including, ATP and capture strand were added to wells. After 15 min incubation at RT fluorescence signal is detected at Ex/Em of 531/590 nm using a PerkinElmer EnVision multimode microplate reader (2103 EnVision™ HTS Microplate Imager, PerkinElmer, USA).

The final concentrations of assay components were: 0.6 μM dsDNA substrate; 1.8 μM capture strand, 30 nM SARS-CoV-2 helicase, 1 mM ATP, 20 μM compound; and 0.2 % DMSO in a total volume of 10 μL/well. The final concentrations of assay components for measurements in presence of 2 mM DTT were: 0.6 μM dsDNA substrate; 1.8 μM capture strand, 3 nM SARS-CoV-2 helicase, 1 mM ATP, 20 μM compound; and 0.2 % DMSO in a total volume of 10 μL/well.

2.4. Helicase NTPase-activity assay

The Promega ADP-Glo Max Assay (#V7001) luciferase-based readout was used to determine the helicase's NTPase activity by measuring the hydrolysis of ATP to ADP during the unwinding of the dsDNA substrate. The assay was performed in 384-well assay microplates (Corning® Low Volume 384-well White Flat Bottom Polystyrene NBS Microplate, #3824) according to the manufacturer's protocol. 20 nL/well of test compounds, positive (20 μM suramin) and negative (100 % DMSO) controls, were transferred by acoustic dispensing (Echo 550R, Labcyte Inc., San José, CA, USA). SARS-CoV-2 nsp13 was diluted in assay buffer, 2.5 μL/well were added to wells and incubated with compounds and controls for 20 min at RT. By the end of incubation time, 2.5 μL/well ATP or ATP including the annealed dsDNA substrate and capture strand were added to the wells. After 15 min incubation at RT, 5 μL/well of ADP-Glo Max Reagent (supplied in the kit) were added to the wells and incubated for 40 min at RT, followed by addition of 10 μL/well detection reagent (supplied in the kit) and an incubation time of 60 min at RT. Luminescence signal was detected using the PerkinElmer EnVision multimode microplate (2103 EnVision™ HTS Microplate Imager, PerkinElmer, USA).

To exclude any unspecific inhibition of the luciferase used in the ADP-Glo Max Assay kit, we retested the compounds in a reference luciferase assay. CellTiter-Glo® Luminescent Cell Viability Assay (#G7570) was adapted to measure changes in Firefly-Luciferase activity. First the sensitivity range of the assay was determined with 1 μM ATP in assay concentration. 10 nL/well of test compounds or DMSO were transferred by acoustic dispensing (Echo 550R, Labcyte Inc., San José, CA, USA) in 384-well assay microplates (Corning® Low Volume 384-well White Flat Bottom Polystyrene NBS Microplate, #3824), 5 μL of CellTiter-Glo® detection reagent was added to compounds and incubated for 20 min at RT. ATP was diluted to 2 μM in assay buffer

containing 0.01 % Tween® 20, 5 μL were added per well. Luminescence signal was detected using the PerkinElmer EnVision multimode microplate reader after 15 min of incubation at RT.

2.5. dsDNA intercalation assay

Quant-iT™ PicoGreen™ Assay (Invitrogen, P7589) was used to detect "biologically interfering" compounds intercalating in the dsDNA substrate. 20 nL/well of test compounds, positive (3.2 μM Hoechst) and negative (100 % DMSO) controls, were transferred by acoustic dispensing (Echo 550R, Labcyte Inc., San José, CA, USA) into 384-well assay microplates (Corning® Low Volume 384-well Black Flat Bottom Polystyrene NBS Microplate, #3820). 25 nM annealed dsDNA substrate diluted in 10 mM Tris–HCl pH 7.4 1 mM EDTA buffer were added to wells. Plates were incubated for 20 min at RT, fluorescence signal was detected using a PerkinElmer EnVision multimode microplate reader at Ex/Em = 485/535 nm.

2.6. Helicase interference assay

Compounds quenching the fluorescence signal of the Cy3-labeled strand and therefore appearing as false positives were excluded from further testing by monitoring their interference at Ex/Em = 531/590 nm. 20 nL/well of test compounds, positive (20 μM suramin) and negative (100 % DMSO) controls, were transferred by acoustic dispensing (Echo 550R, Labcyte Inc., San José, CA, USA) into 384-well assay microplates (Corning® Low Volume 384-well Black Flat Bottom Polystyrene NBS Microplate, #3820). Cy3-labeled DNA strand was diluted in assay buffer (20 mM Tris–HCl pH 7.2, 50 mM NaCl, 5 mM $MgCl_2$) containing 0.01 % Tween®20 and 1 mM ATP and added to each well. After 15 min incubation at RT fluorescence signal was detected using the PerkinElmer EnVision microplate reader (2103 EnVision™ HTS Microplate Imager, PerkinElmer, USA).

2.7. Protein-compound binding assay

SARS-CoV-2 helicase (1.5 μM) and RdRp complex (0.5 μM) were diluted in corresponding assay buffer used in the biochemical assays. The compounds were tested at 20 μM and 100 μM (10 μL total assay volume). Protein samples and compounds were pre-incubated for 30 min before being loaded into Prometheus High Sensitivity Capillaries (NanoTemper Technologies, Munich, Germany) and then heated at rate of 1 °C per minute in the temperature range of 25 to 90 °C (adapted to the melting temperature of nsp13 and nsp12) (Mickolajczyk et al., 2021; Peng et al., 2020). All measurements were performed in triplicates using the Prometheus Panta (NanoTemper Technologies, Munich, Germany). For melting temperature estimation, the "Equilibrium Two State" fitting model of MoltenProt online tool (https://spc.embl-hamburg.de/) was used.

2.8. Data analysis

Analysis of assay development results and dose dependent inhibition curves was performed using GraphPad Prism 8. Dose dependent inhibition curves were fitted using the Variable slope (four parameters) analysis. Compound screening results were analysed with Activitybase (IDBS). Test compound data were normalised relative to respective controls and control well outliers eliminated according to the three-sigma method. Spotfire Analyst 7.11 (TIBCO) was used for visualization/selection.

3. Results

3.1. Assay optimization

One of the main difficulties in developing high-throughput screening (HTS) assays for SARS-CoV-2 RdRp as an isolated protein, is its limited enzymatic activity (Peng et al., 2020), since only in the presence of nsp7 and nsp8 is a fully active replication complex formed (Peng et al., 2020). Here we report the development of a combined in vitro biochemical assay to address enzymatic activity of the RdRp complex by monitoring formation of a generated dsRNA product using Quant-iT™ PicoGreen™. Quant-iT™ PicoGreen™ was originally developed to detect dsDNA molecules, but was also shown to discriminate between dsRNA and ssRNA strands (Eltahla et al., 2013). We used the ability of RdRp to start *de novo* polymerisation synthesis and applied a poly-U ssRNA as oligonucleotide template and ATP as corresponding nucleoside triphosphate (Fig. 1).

The FRET-assay to monitor the unwinding activity of SARS-CoV-2 helicase is based on the enzymes ability to open dsDNA fragments (Fig. 1). The substrate consists of two DNA strands, a leader strand labelled with a 3′-Cyanine-3 fluorophore and the second strand containing a 5′-BHQ-2 quencher. Rebinding of the quencher-labelled strand to the fluorophore strand is ensured by addition of an unlabelled fragment coding for the corresponding region of the quencher-strand. The Promega ADP-Glo Max Assay was used to measure the NTPase activity of helicase, the ADP generated in the hydrolysis of ATP during the unwinding of the dsDNA substrate is quantified to determine the compound effect on the NTPase and unwinding functions of nsp13.

At first, both assays were optimized to meet the quality criteria for a HTS-compatible assay, including DMSO tolerance, statistical performance of controls (Z'), and spatial and temporal uniformity (Gribbon et al., 2005).

3.1.1. Assay optimization for RdRp-complex

Previously, it was shown that SARS-CoV RdRp activity is manganese (Mn^{2+})-dependent, so we evaluated the effects of both 2.5 mM Mn^{2+} and 2.5 mM Mg^{2+} on the RdRp unwinding function (Kirchdoerfer and Ward, 2019; te Velthuis et al., 2010). In the presence of Mg^{2+} we observed a rapid signal increase starting after 30 min of incubation using 300 nM nsp12 and 900 nM nsp7/8, while in combination with Mn^{2+} or in buffer with Mn^{2+} alone, we observed a lowered signal (Suppl. Fig. 5). Titration of oligo-U template and ATP revealed apparent K_{mapp} values of 7.9 μM and 102.7 μM, respectively (Suppl. Fig. 5). Next, we tested inhibition of RdRp using suramin and compared it to competitive action of the dNTP-mix. For suramin, we determined an IC_{50} of 0.67 μM which is in line with the reported IC_{50} of 0.26 μM in a gel-based assay using 3.0 μM poly-A template–primer RNA as substrate (Yin et al., 2021). The IC_{50} for the dNTP-mix was 35.5 μM, in-line with the required half-maximum concentration of dATP necessary to compete the 100 μM ATP present in the assay.

3.1.2. Assay optimization for helicase

To optimize the dsDNA substrate conditions, the helicase was incubated with increasing concentrations of annealed substrate (with capture strand in a ratio of 1:3) at a constant ATP concentration of 2 mM, giving an apparent K_{mapp} of 4.4 μM (Suppl. Fig. 6). In the absence of capture strand (0x), rebinding of the quencher-labelled strand to the fluorophore-labelled strand occurred, leading to a loss of signal (Suppl. Fig. 6). Addition of excess capture strand (>1.25 fold) to the dsDNA annealed substrate prevented rebinding (Suppl. Fig. 6). The helicase was incubated with increasing ATP (at constant dsDNA substrate and capture strand concentrations) to optimize the required ATP concentration, giving an apparent K_{mapp} of 1.9 mM (Suppl. Fig. 6). As helicase was reported to show NTPase activity in absence of an oligonucleotide substrate, we used ADP detection to monitor the consumption of ATP by helicase (Adedeji et al., 2014). Helicase was incubated in presence or absence of dsDNA substrate with increasing concentrations of ATP. An intrinsic basal ATPase activity was observed, the presence of the oligonucleotide substrate enhanced this activity. The results showed higher sensitivity and maximum response for ATP in presence of the dsDNA substrate (Suppl. Fig. 6). We evaluated the effect of reducing

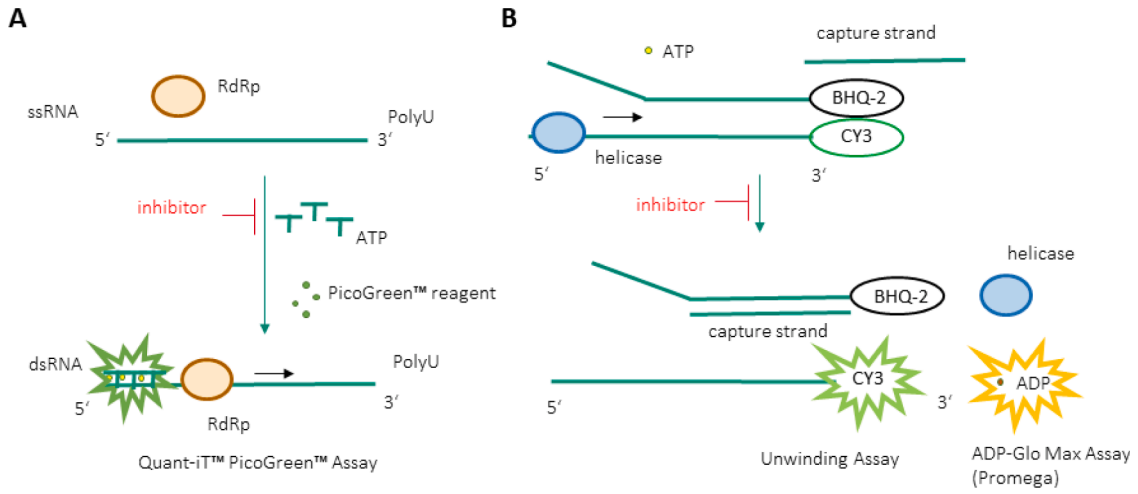

Fig. 1. Schematic overview of RdRp-nsp12/7/8 complex (A) and helicase-nsp13 (B) assays.

conditions/DTT on the kinetic parameters of helicase activity since preliminary studies showed loss of enzyme activity at longer incubation times (Suppl. Fig. 7). In the unwinding assay, the addition of DTT did not result in changes in the K_{mapp} of the dsDNA substrate but, caused an increase in V_{max}, leading to faster turnover of the substrate (Fig. 2). Whereas for ATP hydrolysis, DTT decreased the Km from 1.9 μM to 0.22 μM indicating a potential assay sensitivity to the oxidation-state of the NTPase domain (Fig. 2). We observed no significant effect of addition of the RdRp-complex or single nsps on the helicase activity (Suppl. Fig. 6).

We evaluated suramin and SSYA10-001 in the unwinding and NTPase assay (Fig. 3) (Adedeji et al., 2014; Zeng et al., 2021). Compounds were pre-incubated with helicase for 20 min at RT prior to addition of dsDNA substrate and ATP. We observed that 2 mM DTT effectively eliminated the inhibition of helicase unwinding activity by SSYA10-001, although, previously, inhibition by this compound in the presence of DTT was described (Adedeji et al., 2012). The same observation was made in the NTPase assay. In our hands, SSYA10-001 inhibits NTPase activity only in the absence of DTT (Fig. 3), while the inhibition potency of this compound was enhanced in presence of the dsDNA substrate (Fig. 3). Suramin showed inhibition in absence of DTT, independent of the presence of the dsDNA substrate. Whereas, in presence of 2 mM DTT, the same compound was only active in presence of dsDNA substrate (Fig. 3). Taking into account the observed effects on SSYA10-001 instability in presence of DTT, suramin was selected as the positive control for the primary screen.

3.2. Primary screening

We screened the Fraunhofer Repurposing Collection consisting of 5632 compounds (Kuzikov et al., 2021). Compounds were pre-incubated with RdRp (construct containing SARS-CoV nsp8 and SARS-CoV-2 nsp12 and nsp7- see Material and Methods) or helicase at 20 μM for 20 min at RT followed by addition of the corresponding substrate and detection reagents. Compounds that immediately increased or reduced fluorescence signal at t0 were invalidated as quenching/auto-fluorescent. To identify compounds interfering with the dsDNA/ dsRNA substrate/-product, the Quanti-iT™ PicoGreen™ displacement assay was performed using an annealed dsDNA-fragment. Compounds reducing the Quanti-iT™ PicoGreen™ signal by >40 % were designated as DNA-intercalators and removed from the hit selection process. Three main groups of inhibitors were identified in the combined analysis of RdRp and helicase primary screen: a) compounds inhibiting only RdRp, b) compounds inhibiting only the helicase unwinding activity and c) compounds inhibiting RdRp and helicase unwinding activity (Suppl. Fig. 8). The majority of apparently "dual inhibition" compounds showed intercalating effect in the PicoGreen™ displacement assay (Suppl. Fig. 8; summary of all data can be found in "RdRp_Helicase_SuppFile").

3.3. Hit profiling of compounds with selective RdRp inhibition properties

Compounds were nominally designated as RdRp-selective if: RdRp inhibition >70 %, helicase inhibition <40 %, Quanti-iT™ PicoGreen™ displacement <40 %, and fluorescence interference <40 %. Some 19

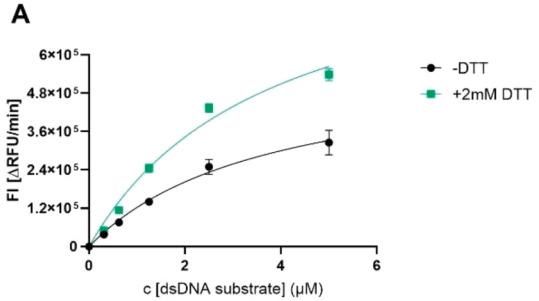

	- DTT	+ 2mM DTT
V_{max} (ΔRFU/min)	581169	989452
K_{mapp} (μM)	3.743	3.769

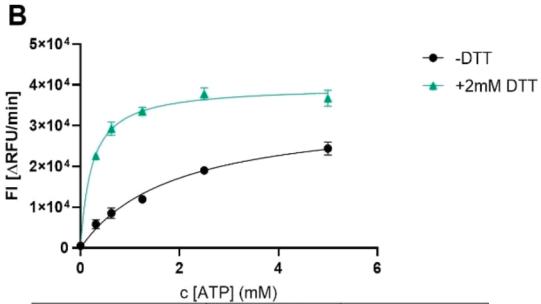

	- DTT	+ 2mM DTT
V_{max} (ΔRFU/min)	33451	39691
K_{mapp} (mM)	1.904	0.228

Fig. 2. Effect of DTT on key kinetic parameters of nsp13. A) Determination of Km and Vmax with respect to dsDNA substrate B) Determination of Km and Vmax with respect to ATP. (Each data point represents $N = 3$, error bars ± SD).

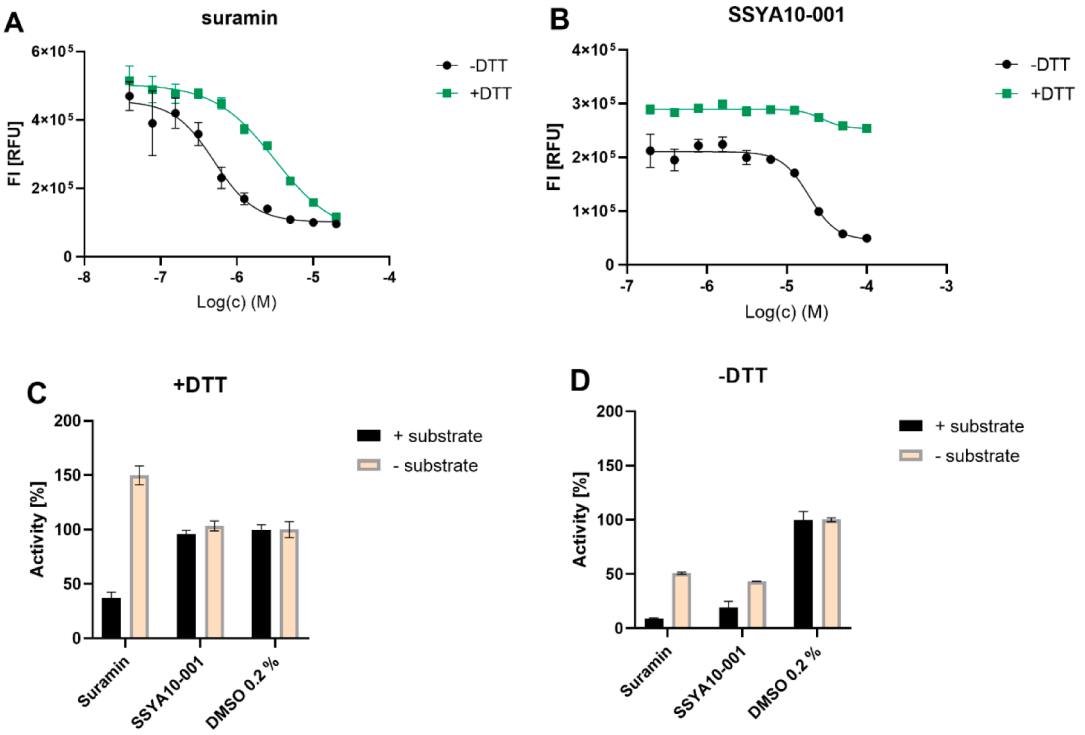

Fig. 3. Inhibition of helicase using reported inhibitors. Inhibition of helicase by suramin A) and SSYA10-001 B) detected in presence and absence of DTT using the unwinding FRET assay. Inhibition of helicase NTPase activity using reported inhibitors suramin C) and SSYA10-001 D) in presence and absence of 2 mM DTT and in presence and absence of the dsDNA substrate. Activity values are normalized to the DMSO control representing conditions with 100 % enzyme activity. (Each data point represents $N = 3$, error bars ± SD).

compounds fulfilled these criteria and 18 compounds were confirmed in hit profiling dose responses (Table 1).

3.4. Hit profiling of compounds with selective helicase inhibition properties

From the helicase primary screen, 84 compounds showing >70 % inhibition of helicase activity and <40 % inhibition of RdRp activity were selected for further investigations. Compounds interfering with the Cy3 dye fluorescence (>40 %) were removed from analysis. Due to putative influence of DTT on compound and NTPase activity, hits were re-tested in presence and absence of DTT. Only seven compounds-maintained inhibition of >50 %: FPA-124, silver sulfadiazine, cardiogreen, opicapone, exifone, plicamycin (mithramycin), aurothioglucose. However, in dose response studies only cardiogreen and plicamycin retained the potency independently of the presence of DTT, while the other compounds demonstrated a substantial increase in IC_{50} value with the addition of DTT (Table 2). In contrast, we observed a lowered IC_{50} value for exifone in presence of 2 mM DTT. To assess whether the inhibitory effect is due to interference with the unwinding or the

Table 1
Hit profiling of RdRp inhibitors.

Compound name	RdRp Inhibition [%] 20 μM	RdRp IC_{50} [μM]	Helicase Inhibition [%] 20 μM	PicoGreen™ effect [%] 20 μM	Interference* [% of control] 20 μM
2-TEDC	97.86	7.99	8.66	7.15	73.21
dynasore	96.07	6.22	7.02	6.63	68.86
nifursol	100.32	11.5	5.5	8.54	71.57
dequalinium chloride	94.6	4.07	25.55	−4.04	82.89
olsalazine sodium	84.71	14.36	5.46	12.75	67.83
eltrombopag olamine	95.18	4.29	3.09	21.05	85.41
rose-bengal-lactone	99.44	n.t.	−2.61	35.69	125.41
PD-118057	81.81	>20	7.76	11.19	87.99
rose bengal sodium salt	97.95	>20	21.51	30.91	153.6
fisetin (fustel)	95.85	2.17	39.32	4.99	65.85
TW-37	89.4	13.65	3.76	3.9	68.91
ethacridine lactate	80.32	9.96	35.49	32.09	87.66
tyrphostin-AG-835	84.15	9.64	7.56	11.5	69
morin hydrate (aurantica)	95.67	5.96	39.33	20.36	78.06
hydroxyzine pamoate	76.75	16.48	4.28	1.28	89.91
primaquine phosphate	102.12	6.56	7.17	1.58	89.41
methacycline hydrochloride	120.03	6.43	25.24	25.54	76.63
oxytetracycline	100.35	16.1	16.36	19.99	76.89

Dose response tests were performed in triplicates using a 1:3 dilution series of compounds; n.t.: not tested.
* Calculated as % of DMSO control signal, DMSO control set to 100 % signal = no interference.

Table 2
Hit profiling of identified helicase inhibitors in the unwinding assay in presence and absence of DTT.

Compound name	Helicase Inhibition [%] 20 μM	IC_{50} [μM]	DTT nsp13 inhibition [%] 20 μM	DTT IC_{50} [μM]	RdRp Inhibition [%] 20 μM	ATPase inhibition [%] 20 μM	PicoGreen™ effect [%] 20 μM	Interference [%] 20 μM
FPA-124	101.03	0.13	64.76	16.89	7.70	106.40	−3.30	1.31
silver sulfadiazine	101.04	1.17	67.30	7.14	−8.87	106.84	0.87	6.68
cardiogreen	100.64	3.57	94.06	3.85	4.44	97.11	26.52	5.04
opicapone	93.61	1.10	51.40	25.49	17.89	96.93	6.86	11.14
exifone	100.3	2.25	101.05	0.29	36.63	104.04	8.87	6.79
plicamycin (Mithramycin)	95.78	3.57	98.09	1.35	6.39	19.77	−3.94	7.18
aurothio-glucose	100.73	1.95	98.65	10.58	4.77	106.07	13.9	4.22

Dose response tests were performed in triplicates using a 1: 3dilution series of compounds.

NTPAse activity of helicase, we tested the confirmed hits in the NTPase assay at 20 μM. All compounds except plicamycin showed a positive correlation between inhibition of the NTPase and unwinding activities at 20 μM (Table 2).

As we previously observed for suramin, the presence of the dsDNA substrate under DTT-conditions may influence the NTPase activity of the helicase. We evaluated cardiogreen, plicamycin and exifone at 2.5 μM (in the range of the calculated IC_{50}) in the NTPase assay in the presence of the dsDNA substrate and 2 mM DTT. Cardiogreen and exifone showed positive correlation between unwinding and NTPase inhibition. Inhibition by plicamycin was not observed in the NTPase assay, whereby addition of the dsDNA substrate did not result in changes of observed effect (Table 3). Plicamycin (mithramycin) was the only compound with 72 % inhibition (in the unwinding assay at 2.5 μM and no effect on the NTPase 114.6 %). Cardiogreen demonstrated a similar potency at 2.5 μM in both assays, showing 65 % inhibition in the unwinding assay, and 60.4 % remaining NTPase activity. Exifone showed strong inhibition at 2.5 μM in both assays: 99.9 % in the unwinding assay and 14.5 % remaining NTPase activity.

3.5. Hit profiling of compounds with dual-inhibition properties

In order to target both viral proteins, RdRp and helicase, in the replication process and thus to interfere on multiple steps with viral infection, we selected compounds with dual-inhibition potency against RdRp and helicase. From the primary screen we selected only those helicase hits which showed no sensitivity towards DTT, as DTT was present in the RdRp primary screen. Compounds were identified as hits when they showed >50 % inhibition against both target proteins in presence of DTT. The interference cut-off was defined as <40 % effect in the Quanti-iT™ PicoGreen™ displacement assay, <40 % in the helicase interference assay, and <40 % in the RdRp interference at t0. Four hits were identified: disodium 7,7′-(carbonyldiimino) bis(4-hydroxy-2-naphthalenesulfonate) (AMI-1), suramin hexasodium, (-)-epigallocatechin gallate, myricetin (cannabiscetin). For characterization of helicase inhibition towards its unwinding and NTPase function, we used the same criteria as described above.

We confirmed suramin dual-inhibition for RdRp and helicase, and again we observed inhibition of the helicase NTPase activity only in presence of dsDNA substrate (in presence of 2 mM DTT). For disodium 7,7′-(carbonyldiimino) bis(4-hydroxy-2-naphthalenesulfonate) (AMI-1), (-)-epigallocatechin gallate and myricetin (Cannabiscetin), we observed positive correlation between inhibition of the helicase NTPase and unwinding activity. To assess selectivity of the identified hits towards RdRp or helicase, we tested them in dose response (Suppl. Fig. 9). For disodium 7,7′-(carbonyldiimino) bis(4-hydroxy-2-naphthalenesulfonate) (AMI-1) no clear preference was observed, whereas suramin demonstrated stronger potency against RdRp (IC_{50} 0.24 μM) as compared to the helicase (IC_{50} 5.42 μM) (Table 4). In contrast (−)-epigallocatechin gallate showed stronger inhibition of the helicase (IC_{50} 0.38 μM) compared to RdRp (IC_{50} > 20 μM) (Table 4). For myricetin (Cannabiscetin) a slight preference towards RdRp was observed with a RdRp (IC_{50} 0.86 μM) compared to the helicase (IC_{50} 4.14 μM) and a maximal response of 100.7 % inhibition of RdRp compared to 67.25 % helicase inhibition.

3.6. Confirmation of inhibitor binding

To show a direct compound with target-protein interaction, Tm determination using nano differential scanning fluorimetry (nDSF) was performed. Eltrombopag olamine, fisetin and dynasore were selected as putative RdRp selective compounds. Exifone, plicamycin (mithramycin) and (−)-epigallocatechin gallate were selected as helicase selective. Suramin hexasodium and myricetin were selected as dual-active helicase and RdRp inhibitors (Suppl. Fig. 10). As for the inhibition assays, incubation of compounds and proteins was performed in absence of the substrates. Compound effects on protein thermal stability were measured at 20 μM and 100 μM after 30 min incubation with helicase or RdRp (Table 5). For RdRp we observed an increase in melting temperature for suramin hexasodium, and the effect was concentration dependent. Dynasore increased the Tm of RdRp by about 1.5 K at 100 μM compound concentration, from 43 °C to 44.5 °C. For helicase we observed a decrease in Tm caused by suramin hexasodium and exifone, whereby the effect of exifone was only detected at 100 μM. In addition, we observed a shift of helicase Tm to higher values when incubating the enzyme with a higher DMSO concentration (from 0.2 % to 1 %) (Table 5).

To investigate whether we can observe a competitive mode of action of suramin and dynasore in regards of increasing ATP/oligoU concentration, we tested the inhibitors in dose response in the presence of increasing concentration of substrates. We observed no changes in IC_{50}

Table 3
Hit profiling of selected helicase inhibitors in the ATPase assay in presence and absence of the dsDNA substrate and DTT.

Compound name	Helicase unwinding inhibition 2.5 μM triplicates	Helicase ATPase activity [%] 2 μM	Helicase ATPase activity PLUS DNA substrate 2 μM	DTT Helicase unwinding inhibition [%] 2.5 μM triplicates	DTT Helicase ATPase activity [%] 2 μM	DTT Helicase ATPase activity PLUS DNA substrate 2 μM
cardiogreen	66.59	45.65	32.88	65.01	60.43	51.49
exifone	49.85	11.33	4.96	99.91	14.53	2.64
plicamycin (mithramycin)	38.98	125.71	159.86	71.99	114.66	133.03

Dose response tests were performed in triplicates using a 1:3 dilution series of compounds.

Table 4
Hit profiling of identified dual-active compounds against RdRp and helicase.

Compound name	RdRp Inhibition [%] 20 μM	RdRp IC_{50} μM	Helicase Inhibition [%] 20 μM	DTT Helicase Inhibition [%] 20 μM	DTT Helicase IC_{50} μM	DTT Helicase Inhibition [%] 2.5 μM	DTT Helicase ATPase activity [%] 2 μM	DTT Helicase ATPase activity PLUS DNA substrate 2 μM
disodium 7,7′-(carbonyldiimino) bis(4-hydroxy-2-naphthalenesulfonate)	90.5	>20	84.75	65.72	>20	6.27	103.17	103.05
suramin hexasodium	98.49	0.24	97.97	92.60	5.42	53.07	121.61	63.38
(−)-epigallocatechin gallate	85.49	>20	96.39	78.10	0.38	73.51	43.42	31.66
myricetin (cannabiscetin)	100.7	0.86	100.46	67.25	4.14	22.05	62.36	77.50

Dose response tests were performed in triplicates using a 1: 3dilution series of compounds.

Table 5
Tm determination of RdRp and helicase in presence of selected inhibitors using nDSF.

Compound name	Helicase				RdRp			
	Tm °C (±SD) 20 μM*		Tm °C (±SD) 100 μM**		Tm °C (±SD) 20 μM		Tm °C (±SD) 100 μM	
eltrombopag olamine	n.t.		n.t.		41.5	1.1	43.6	0.8
fisetin (fustel)	n.t.		n.t.		42.7	0.2	43.5	0.5
suramin hexasodium	36.8	0.1	36.5	0.1	44.3	1.0	46.6	0.4
myricetin (cannabiscetin)	38.3	0.2	38.8	0.1	42.7	0.4	43.6	0.5
dynasore	n.t.		n.t.		43.3	0.3	44.5	0.4
exifone	38.3	0.2	37.8	0.1	n.t.		n.t.	
plicamycin (mithramycin)	38.3	0.3	38.9	0.0	n.t.		n.t.	
(−)-epigallocatechin gallate	38.4	0.5	39.6	0.1	n.t.		n.t.	
DMSO (0.2 %* or 1 %**)	38.2	0.3	39.0	0.0	42.8	0.4	43.0	0.1

n.t.: not tested.

of suramin in the presence of increasing concentrations of oligo-U or ATP for inhibition of the RdRp. For dynasore, we saw a gain of potency in the presence of 3 μM oligo-U in contrast to 10 μM and 30 μM oligo-U substrate. We did not detect any change due to increasing ATP concentration (Fig. 4).

4. Discussion

The evolution of SARS-CoV-2 in the past three years, which was accompanied by a partial loss of effectiveness of developed vaccines, highlights the increased need for novel antiviral compounds (Lau et al., 2023; Grimes et al., 2023). Due to conservation across coronaviruses and the essential role in progression of infection the RdRp and helicase were considered as promising drug targets from the outset. Therefore, we performed a drug repurposing screening approach in order to identify compounds inhibiting each single and/or both proteins. We identified three groups of hits: compounds inhibiting either the helicase or the RdRp, and compounds addressing both enzymes.

The majority of compounds with dual-activity against helicase and RdRp were invalidated in the counter DNA intercalation assay and

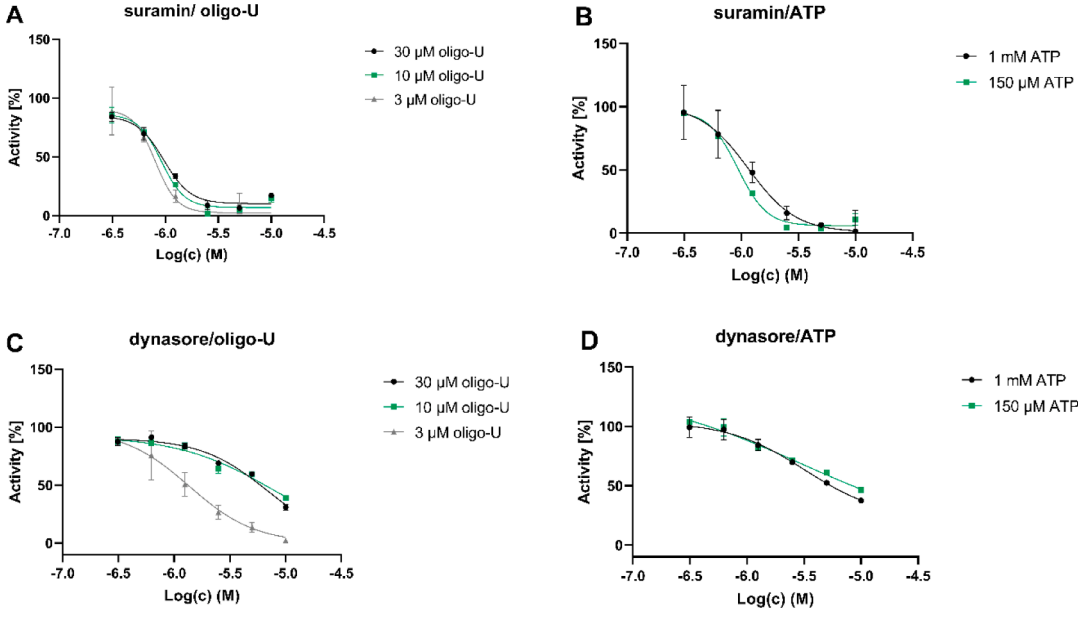

Fig. 4. Dose dependent inhibition of RdRp using suramin and dynasore in presence of increasing concentration of oligo-U substrate and ATP. RdRp was pre-incubated with suramin for 30 min followed by addition of oligo-U substrate A) or ATP B) in increasing concentration. RdRp was pre-incubated with dynasore for 30 min followed by addition of oligo-U substrate C) or ATP D) in increasing concentration. (Each data point represents $N = 3$, error bars ± SD).

fluorescence interference assays, including hemin, hexachlorophene, SRT1720 HCl, and tolonium chloride (Supp. Table-File). Nevertheless, Disodium 7,7′-(carbonyldiimino) bis(4-hydroxy-2-naphthalenesulfonate) (AMI-1), suramin hexasodium, epigallocatechin gallate, and myricetin were identified as dual-active inhibitors at 20 μM. According to the dose response analysis, AMI-1 was equally inhibitory towards both enzymes, although with an $IC_{50} > 20$ μM. AMI-1 was previously described to inhibit HIV-1 reverse transcriptase with an IC_{50} of 5 μM and K_D of 2 μM (Skillman et al., 2002). The proposed mechanism of action proposed is the inhibition of dsDNA binding to the reverse transcriptase of HIV-1 (Skillman et al., 2002). For suramin hexasodium and myricetin we observed a preference of for RdRp inhibition and for epigallocatechin gallate towards nsp13 inhibition.

Besides suramin hexasodium and myricetin, we identified 10 compounds as RdRp inhibitors with an $IC_{50} < 10$ μM: 2-TEDC, dynasore, dequalinium chloride, eltrombopag olamine, fisetin (fustel), ethacridine lactate, tyrphostin-AG-835, morin hydrate (aurantica), primaquine phosphate, methacycline hydrochloride. Previously, dequalinium chloride, ethacridine and eltrombopag olamine were described to inhibit entry of Marburg virus and SARS-CoV-2 (Pubchem, 2023; Feng et al., 2020; li et al., 2021). Myricetin, fisetin (fustel), morin and primaquine phosphate are flavones and flavone-derivatives, a compound class which exhibits activity against a broad range of biological targets, including SARS-CoV-2 (Taldaev et al., 2022; Panche et al., 2016; Wen et al., 2021). In addition, Shiomi et al. reported flavones inhibiting mammalian DNA polymerases and human DNA topoisomerase, with myricetin having an IC_{50} of 27.5 μM (Shiomi et al., 2013). The proposed mechanism of action excluded the myricetin-driven inhibition of polymerase binding to dsDNA (Shiomi et al., 2013). But taking into account that no shift in Tm was observed using nDSF to monitor interaction with RdRp, we cannot exclude unspecific interference with assay components (Kumar and Pandey, 2013). Our nDSF studies demonstrated a concentration-dependent protein stabilizing effect by suramin hexasodium and dynasore. By applying competitive studies to observe inhibition effect of suramin hexasodium and dynasore in presence of increasing concentration of oligo-U or ATP, we saw no competitive effect towards suramin hexasodium for both substrates (Yin et al., 2021). Dynasore showed loss of potency in presence of increased oligo-U concentration, therefore we tend to propose the template-binding pocket as a preferred interaction point of dynasore with RdRp. Dynasore is a well-known GTPase dynamin inhibitor ($IC_{50} = 15$ μM) inhibiting the clathrin-mediated endocytosis (Medchemexpress, 2023). It was reported to disturb traffic of entry of viruses, including herpes simplex virus (HSV) (Mues et al., 2015). We recently reported the preference of the Omicron/BA.1 variant for the endocytotic entry pathway, whereas the D614G variant uses both pathways (Kuzikov et al., 2022). Taking together, the observation from the current screen and reported data on entry inhibition, we can speculate of the possibility for dynasore to target both steps of SARS-CoV-2 infection pathway: entry and replication. On the other hand, correlating the observed enzymatic inhibition of identified hits with the results obtained in our in-house SARS-CoV-2 infection assay in VeroE6 cells, we saw limited correlation (Suppl. Table 1), (Zaliani et al., 2022). Considering the compounds' metabolic stability after 48 h incubation, as used with the cell in the CPE assay, or their effects on PgP-driven efflux pumps and their poor passive membrane penetration, such as suramin, we can't exclude that the minimal observed compound CPE effects are due to their reduced in-cell concentration (Sanderson et al., 2007). In addition, as shown for suramin analogues, onset of intracellular compound activity occurs at over 100-fold excess of the identified IC_{50} in biochemical assays (Yin et al., 2021). Thus, we can't exclude intracellular activity and aim for re-evaluation of identified hits in the future.

For determination of helicase inhibition, we monitored both unwinding and inhibition of the ATPase activity. We noticed high sensitivity of the helicase towards the presence of DTT reducing agent, especially in the NTPase assay. Most primary screening hits (no DTT present) lost their inhibition capacity when retested in the presence of 2 mM DTT, potentially due to a reactive mode of action and enhanced helicase stabilisation under reducing conditions as observed during assay development for the NTPase activity (Supp. Fig. 7). For epigallocatechin gallate, cardiogreen, suramin, disodium 7,7′-(carbonyldiimino) bis(4-hydroxy-2-naphthalenesulfonate), myricetin, and plicamycin enzyme inhibition at 20 μM was largely independent of presence of DTT. For exifone we saw a strong gain of compound potency in presence of DTT. Being a member of the benzophenone class of molecules it is used as a photo crosslinking probe upon reaction under UV-light, generating free radicals (Kecici et al., 2018). It can react with a hydrogen donor molecule, such as thiol present in DTT, that is acting as co-initiator of the photo crosslinking, promoting the reaction. During assay adaptation we confirmed the previously described intrinsic basal ATPase activity of helicase, which increased in presence of a dsDNA substrate (de Wit et al., 2016; Sawicki and Sawicki, 1995). The majority of identified inhibitors showed positive correlations between inhibition of intrinsic basal ATPase activity and inhibition of unwinding activity. The findings support previous studies reporting on compounds interfering with the NTPase activity of helicase which did not primarily inhibit the unwinding activity (Spratt et al., 2021; Yu et al., 2012). Suramin and plicamycin showed, however, selective inhibition of the unwinding activity. Whereby, ATPase inhibition by suramin occurred after addition of the dsDNA substrate and plicamycin activity was substrate-independent. For epigallocatechin gallate, exifone, and cardiogreen we observed a small gain of ATPase activity reduction (10–15 %) in the presence of dsDNA substrate. In assessing helicase-compound interactions through nDSF studies, we observed destabilizing effects of suramin hexasodium and exifone, most probably caused by unspecific destabilisation of the enzyme, supporting the reported mode of action of exifone through radical formation (Kecici et al., 2018). Incubation of the helicase with epigallocatechin gallate, myricetin, and plicamycin did not result in a Tm change. For plicamycin we saw a competitive mode of inhibition towards the dsDNA substrate and no effect of increasing ATP concentration (Suppl. Fig. 11). Taking into consideration published data on minor groove binding properties of plicamycin and no detectable Tm shift, we assume an unspecific interaction with the dsDNA substrate making it unavailable for helicase in assay and therefore, appearing as a false positive hit (Barceló et al., 2010). But also, for helicase inhibitors identified in this study, we saw limited effect in the in-house SARS-CoV-2 CPE infection assay (Suppl. Table 1), (Zaliani et al., 2022).

5. Conclusion

Our study demonstrates a combined screening approach targeting key functions of the SARS-CoV-2 replication and transcription complex. Our strict screening cascade invalidated false positives through a combination of orthogonal assays and resulted in starting points for the development of new inhibitors. We have successfully confirmed the activity of suramin hexasodium against the SARS-CoV-2 RdRp complex and identified dynasore as a novel potent inhibitor. Additionally, we have revealed the destabilizing properties of suramin hexasodium and exifone on SARS-CoV-2 helicase, confirming the challenges in finding specific inhibitors for this target. Moving forward, it might be necessary to develop novel combinational approaches that also consider new modulation strategies, such as protein-protein interaction inhibitors, to identify specific inhibitors that target key factors involved in viral replication machinery and maybe overcome compound promiscuity for this target class. These efforts can advance the development of promising therapies.

CRediT authorship contribution statement

Maria Kuzikov: Writing – original draft, Visualization, Validation, Methodology, Investigation, Formal analysis, Conceptualization. **Jeanette Reinshagen:** Formal analysis, Data curation. **Krzysztof Wycisk:** Writing – review & editing, Resources. **Angela Corona:** Methodology. **Francesca Esposito:** Methodology. **Paolo Malune:** Methodology.

Candida Manelfi: Conceptualization. **Daniela Iaconis:** Writing – review & editing, Conceptualization. **Andrea Beccari:** Conceptualization. **Enzo Tramontano:** Writing – review & editing, Conceptualization. **Marcin Nowotny:** Writing – review & editing, Conceptualization. **Björn Windshügel:** Writing – review & editing, Supervision. **Philip Gribbon:** Writing – review & editing, Supervision, Project administration, Funding acquisition, Conceptualization. **Andrea Zaliani:** Writing – review & editing, Supervision, Project administration, Conceptualization.

Declaration of competing interest

The authors declare that they have no known competing financial interests or personal relationships that could have appeared to influence the work reported in this paper.

Data availability

Data can be found in the supplementary file.

Acknowledgements

Exscalate4Cov financed this study under the European Union's Horizon 2020 Research and Innovation Programme (grant agreement no 101003551). Data release and preparation was funded by under H2020 projects EOSC-LIFE (grant agreement number 824087) and BY-COVID (grant agreement number 101046203). We thank Emma Manners, Anna Gaulton and Andrew Leach at ChEMBL for excellent support in organising data sets. We thank Yulia Gerhardt and Peter Maas of SPECS and Joshua Bitker (ex-Broad) for input into the selection and quality control of the Fraunhofer compound library. We acknowledge technical support by the SPC facility at EMBL Hamburg.

Supplementary materials

Supplementary material associated with this article can be found, in the online version, at doi:10.1016/j.virusres.2024.199356.

References

Adedeji, A.O., Singh, K., Calcaterra, N.E., DeDiego, M.L., Enjuanes, L., Weiss, S., Sarafianos, S.G., 2012. Severe acute respiratory syndrome coronavirus replication inhibitor that interferes with the nucleic acid unwinding of the viral helicase. Antimicrob. Agents Chemother. 56 (9), 4718–4728. https://doi.org/10.1128/AAC.00957-12.

Adedeji, A.O., Singh, K., Kassim, A., Coleman, C.M., Elliott, R., Weiss, S.R., Frieman, M. B., Sarafianos, S.G., 2014. Evaluation of SSYA10-001 as a replication inhibitor of severe acute respiratory syndrome, mouse hepatitis, and Middle East respiratory syndrome coronaviruses. Antimicrob. Agents Chemother. 58 (8), 4894–4898. https://doi.org/10.1128/AAC.02994-14.

Ahn, D.G., Choi, J.K., Taylor, D.R., Oh, J.W., 2012. Biochemical characterization of a recombinant SARS coronavirus nsp12 RNA-dependent RNA polymerase capable of copying viral RNA templates. Arch. Virol. 157 (11), 2095–2104. https://doi.org/10.1007/s00705-012-1404-x.

Barceló, F., Ortiz-Lombardía, M., Martorell, M., Oliver, M., Méndez, C., Salas, J.A., Portugal, J., 2010. DNA binding characteristics of mithramycin and chromomycin analogues obtained by combinatorial biosynthesis. Biochemistry 49 (49), 10543–10552. https://doi.org/10.1021/bi101398s.

Corona, A., Wycisk, K., Talarico, C., Manelfi, C., Milia, J., Cannalire, R., Esposito, F., Gribbon, P., Zaliani, A., Iaconis, D., Beccari, A.R., Summa, V., Nowotny, M., Tramontano, E., 2022. Natural compounds inhibit SARS-CoV2 Nsp13 unwinding and ATPase enzyme activities. ACS Publ. J. Contrib. https://doi.org/10.1021/acsptsci.1c00253.s001.

Covariants, 2023 https://covariants.org/variants/21K.Omicron. 05.07.2023.

de Wit, E., van Doremalen, N., Falzarano, D., Munster, V.J., 2016. SARS and MERS: recent insights into emerging coronaviruses. Nat. Rev. Microbiol. 14, 523–534. https://doi.org/10.1038/nrmicro.2016.81.

Eastman, R.T., Roth, J.S., Brimacombe, K.R., Simeonov, A., Shen, M., Patnaik, S., Hall, M.D., 2020. Remdesivir: a review of its discovery and development leading to emergency use authorization for treatment of COVID-19. ACS Cent. Sci. 6 (5), 672–683. https://doi.org/10.1021/acscentsci.0c00489.

Eltahla, A.A., Lackovic, K., Marquis, C., Eden, J.S., White, P.A., 2013. A fluorescence-based high-throughput screen to identify small compound inhibitors of the genotype 3a hepatitis C virus RNA polymerase. J. Biomol. Screen 18 (9), 1027–1034. https://doi.org/10.1177/1087057113489883.

EMA, 2021 https://www.ema.europa.eu/en/documents/press-release/first-covid-19-treatment-recommended-eu-authorisation_en.pdf. 08.09.2021.

FDA, 2021 https://www.fda.gov/news-events/press-announcements/fda-approves-first-treatment-covid-19. 08.09.2021.

Feng, S., Luan, X., Wang, Y., Wang, H., Zhang, Z., Wang, Y., Tian, Z., Liu, M., Xiao, Y., Zhao, Y., Zhou, R., Zhang, S., 2020. Eltrombopag is a potential target for drug intervention in SARS-CoV-2 spike protein. Infect., Genet. Evol. 85, 104419 https://doi.org/10.1016/j.meegid.2020.104419.

Gorbalenya, A.E., Pringle, F.M., Zeddam, J.L., Luke, B.T., Cameron, C.E., Kalmakoff, J., Hanzlik, T.N., Gordon, K.H., Ward, V.K., 2002. The palm subdomain-based active site is internally permuted in viral RNA-dependent RNA polymerases of an ancient lineage. J. Mol. Biol. 324 (1), 47–62. https://doi.org/10.1016/s0022-2836(02)01033-1.

Gordon, C.J., Tchesnokov, E.P., Feng, J.Y., Porter, D.P., Götte, M., 2020. The antiviral compound remdesivir potently inhibits RNA-dependent RNA polymerase from Middle East respiratory syndrome coronavirus. J. Biol. Chem. 295 (15), 4773–4779. https://doi.org/10.1074/jbc.AC120.013056.

Gribbon, P., Lyons, R., Laflin, P., Bradley, J., Chambers, C., Williams, B.S., Keighley, W., Sewing, A., 2005. Evaluating real-life high-throughput screening data. J. Biomol. Screen 10 (2), 99–107. https://doi.org/10.1177/1087057104271957.

Grimes, S.L., Choi, Y.J., Banerjee, A., Small, G., Anderson-Daniels, J., Gribble, J., Pruijssers, A.J., Agostini, M.L., Abu-Shmaism, A., Lu, X., Darst, S.A., Campbell, E., Denison, M.R., 2023. A mutation in the coronavirus nsp13-helicase impairs enzymatic activity and confers partial remdesivir resistance. MBio, e0106023. https://doi.org/10.1128/mbio.01060-23.

Ivanov, K.A., Thiel, V., Dobbe, J.C., van der Meer, Y., Snijder, E.J., Ziebuhr, J., 2004. Multiple enzymatic activities associated with severe acute respiratory syndrome coronavirus helicase. J. Virol. 78 (11), 5619–5632. https://doi.org/10.1128/JVI.78.11.5619-5632.2004.

Jia, Z., Yan, L., Ren, Z., Wu, L., Wang, J., Guo, J., Zheng, L., Ming, Z., Zhang, L., Lou, Z., Rao, Z., 2019. Delicate structural coordination of the Severe Acute Respiratory Syndrome coronavirus Nsp13 upon ATP hydrolysis. Nucleic Acids Res. 47 (12), 6538–6550. https://doi.org/10.1093/nar/gkz409.

Joshi, S., Parkar, J., Ansari, A., Vora, A., Talwar, D., Tiwaskar, M., Patil, S., Barkate, H., 2021. Role of favipiravir in the treatment of COVID-19. Int. J. Infect. Dis. 102, 501–508. https://doi.org/10.1016/j.ijid.2020.10.069.

Kecici, Z., Babaoglu, S., Temel, G., 2018. Methacrylated benzophone as triple functional compound for the synthesis of partially crosslinked copolymers. Prog. Org. Coat. 415, 138–142. https://doi.org/10.1016/j.porgcoat.2017.11.015.

Kirchdoerfer, R.N., Ward, A.B., 2019. Structure of the SARS-CoV nsp12 polymerase bound to nsp7 and nsp8 co-factors. Nat. Commun. 10, 2342. https://doi.org/10.1038/s41467-019-10280-3.

Kumar, S., Pandey, A.K., 2013. Chemistry and biological activities of flavonoids: an overview. ScientificWorldJournal 2013, 162750. https://doi.org/10.1155/2013/162750.

Kuzikov, M., Costanzi, E., Reinshagen, J., Esposito, F., Vangeel, L., Wolf, M., Ellinger, B., Claussen, C., Geisslinger, G., Corona, A., Iaconis, D., Talarico, C., Manelfi, C., Cannalire, R., Rossetti, G., Gossen, J., Albani, S., Musiani, F., Herzog, K., Ye, Y., Zaliani, A., 2021. Identification of inhibitors of SARS-CoV-2 3CL-pro enzymatic activity using a small molecule in vitro repurposing screen. ACS Pharmacol. Transl. Sci. 4 (3), 1096–1110. https://doi.org/10.1021/acsptsci.0c00216.

Kuzikov, M., Woens, J., Zaliani, A., Hambach, J., Eden, T., Fehse, B., Ellinger, B., Riecken, K., 2022. High-throughput drug screening allowed identification of entry inhibitors specifically targeting different routes of SARS-CoV-2 delta and omicron/BA.1. Biomed. Pharmacother. 151, 113104 https://doi.org/10.1016/j.biopha.2022.113104.

Lau, J.J., Cheng, S.M.S., Leung, K., Lee, C.K., Hachim, A., Tsang, L.C.H., Yam, K.W.H., Chaothai, S., Kwan, K.K.H., Chai, Z.Y.H., Lo, T.H.K., Mori, M., Wu, C., Valkenburg, S. A., Amarasinghe, G.K., Lau, E.H.Y., Hui, D.S.C., Leung, G.M., Peiris, M., Wu, J.T., 2023. Real-world COVID-19 vaccine effectiveness against the Omicron BA.2 variant in a SARS-CoV-2 infection-naive population. Nat. Med. 29 (2), 348–357. https://doi.org/10.1038/s41591-023-02219-5.

Li, X., Lidsky, P.V., Xiao, Y., Wu, C.T., Garcia-Knight, M., Yang, J., Nakayama, T., Nayak, J.V., Jackson, P.K., Andino, R., Shu, X., 2021. Ethacridine inhibits SARS-CoV-2 by inactivating viral particles. PLoS Pathog. 17 (9), e1009898 https://doi.org/10.1371/journal.ppat.1009898.

Madru, C., Tekpinar, A.D., Rosario, S., Czernecki, D., Brûlé, S., Sauguet, L., Delarue, M., 2021. Fast and efficient purification of SARS-CoV-2 RNA dependent RNA polymerase complex expressed in Escherichia coli. PLoS One 16, e0250610.

Malone, B., Urakova, N., Snijder, E.J., Campbell, E.A., 2022. Structures and functions of coronavirus replication-transcription complexes and their relevance for SARS-CoV-2 drug design. Nat. Rev. Mol. Cell Biol. 23 (1), 21–39. https://doi.org/10.1038/s41580-021-00432-z.

Medchemexpress, 2023 https://www.medchemexpress.com/Dynasore.html (06.06.2023).

Mickolajczyk, K.J., Shelton, P.M.M., Grasso, M., Cao, X., Warrington, S.E., Aher, A., Liu, S., Kapoor, T.M., 2021. Force-dependent stimulation of RNA unwinding by SARS-CoV-2 nsp13 helicase. Biophys. J. 120 (6), 1020–1030. https://doi.org/10.1016/j.bpj.2020.11.2276.

Mues, M.B., Cheshenko, N., Wilson, D.W., Gunther-Cummins, L., Herold, B.C., 2015. Dynasore disrupts trafficking of herpes simplex virus proteins. J. Virol. 89 (13), 6673–6684. https://doi.org/10.1128/JVI.00636-15.

Newman, J.A., Douangamath, A., Yadzani, S., Yosaatmadja, Y., Aimon, A., Brandão-Neto, J., Dunnett, L., Gorrie-stone, T., Skyner, R., Fearon, D., Schapira, M., von

Delft, F., Gileadi, O., 2021. Structure, mechanism and crystallographic fragment screening of the SARS-CoV-2 NSP13 helicase. *Nat.* Commun 12, 4848.
Panche, A.N., Diwan, A.D., Chandra, S.R., 2016. Flavonoids: an overview. J. Nutr. Sci. 5, e47. https://doi.org/10.1017/jns.2016.41.
Peng, Q., Peng, R., Yuan, B., Zhao, J., Wang, M., Wang, X., Wang, Q., Sun, Y., Fan, Z., Qi, J., Gao, G.F., Shi, Y., 2020. Structural and biochemical characterization of the nsp12-nsp7-nsp8 core polymerase complex from SARS-CoV-2. Cell Rep. 31 (11), 107774 https://doi.org/10.1016/j.celrep.2020.107774.
Pubchem, 2023 https://pubchem.ncbi.nlm.nih.gov/bioassay/540276#sid=50106101&section=Version, 07.06.2023.
Sanderson, L., Khan, A., Thomas, S., 2007. Distribution of suramin, an antitrypanosomal drug, across the blood-brain and blood-cerebrospinal fluid interfaces in wild-type and P-glycoprotein transporter-deficient mice. Antimicrob. Agents Chemother. 3136–3146. https://doi.org/10.1128/AAC.00372-07. Epub 2007 Jun 18. PMID: 17576845; PMCID: PMC2043191.
Sawicki, S.G., Sawicki, D.L., 1995. Coronaviruses use discontinuous extension for synthesis of subgenome-length negative strands. Adv. Exp. Med. Biol. 380, 499–506. https://doi.org/10.1007/978-1-4615-1899-0_79.
Sheahan, T.P., Sims, A.C., Zhou, S., Graham, R.L., Pruijssers, A.J., Agostini, M.L., Leist, S. R., Schäfer, A., Dinnon 3rd, K.H., Stevens, L.J., Chappell, J.D., Lu, X., Hughes, T.M., George, A.S., Hill, C.S., Montgomery, S.A., Brown, A.J., Bluemling, G.R., Natchus, M. G., Saindane, M., Baric, R.S., 2020. An orally bioavailable broad-spectrum antiviral inhibits SARS-CoV-2 in human airway epithelial cell cultures and multiple coronaviruses in mice. Sci. Transl. Med. 12 (541), eabb5883. https://doi.org/10.1126/scitranslmed.abb5883.
Shiomi, K., Kuriyama, I., Yoshida, H., Mizushina, Y., 2013. Inhibitory effects of myricetin on mammalian DNA polymerase, topoisomerase and human cancer cell proliferation. Food Chem. 139 (1–4), 910–918. https://doi.org/10.1016/j.foodchem.2013.01.009.
Skillman, A.G., Maurer, K.W., Roe, D.C., Stauber, M.J., Eargle, D., Ewing, T.J., Muscate, A., Davioud-Charvet, E., Medaglia, M.V., Fisher, R.J., Arnold, E., Gao, H.Q., Buckheit, R., Boyer, P.L., Hughes, S.H., Kuntz, I.D., Kenyon, G.L., 2002. A novel mechanism for inhibition of HIV-1 reverse transcriptase. Bioorg. Chem. 30 (6), 443–458. https://doi.org/10.1016/s0045-2068(02)00502-3.
Sommers, J.A., Loftus, L.N., Jones 3rd, M.P., Lee, R.A., Haren, C.E., Dumm, A.J., Brosh Jr., R.M., 2023. Biochemical analysis of SARS-CoV-2 Nsp13 helicase implicated in COVID-19 and factors that regulate its catalytic functions. J. Biol. Chem. 299 (3), 102980 https://doi.org/10.1016/j.jbc.2023.102980.
Spratt, A.N., Gallazzi, F., Quinn, T.P., Lorson, C.L., Sönnerborg, A., Singh, K., 2021. Coronavirus helicases: attractive and unique targets of antiviral drug-development and therapeutic patents. Expert Opin. Ther. Pat. 31 (4), 339–350. https://doi.org/10.1080/13543776.2021.1884224.
Subissi, L., Posthuma, C.C., Collet, A., Zevenhoven-Dobbe, J.C., Gorbalenya, A.E., Decroly, E., Snijder, E.J., Canard, B., Imbert, I., 2014. One severe acute respiratory syndrome coronavirus protein complex integrates processive RNA polymerase and exonuclease activities. Proc. Natl. Acad. Sci. USA 111 (37), E3900–E3909. https://doi.org/10.1073/pnas.1323705111.
Taldaev, A., Terekhov, R., Nikitin, I., Zhevlakova, A., Selivanova, I., 2022. Insights into the pharmacological effects of flavonoids: the systematic review of computer modeling. Int. J. Mol. Sci. 23 (11), 6023. https://doi.org/10.3390/ijms23116023.
Tanner, J.A., Watt, R.M., Chai, Y.B., Lu, L.Y., Lin, M.C., Peiris, J.S.M., Poon, L.L.M., Kung, H.-F., Huang, J.-D., 2003. The severe acute respiratory syndrome (SARS) coronavirus NTPase/helicase belongs to a distinct class of 5′ to 3′ viral helicases. J. Biol. Chem. 278, 39578–39582. https://doi.org/10.1074/jbc.C300328200.
te Velthuis, A.J., Arnold, J.J., Cameron, C.E., van den Worm, S.H., Snijder, E.J., 2010. The RNA polymerase activity of SARS-coronavirus nsp12 is primer dependent. Nucleic Acids Res. 38 (1), 203–214. https://doi.org/10.1093/nar/gkp904.
Ulferts, R., Imbert, I., Canard, B., Ziebuhr, J., 2010. Expression and functions of SARS coronavirus replicative proteins. In: Lal, S. (Ed.), Molecular Biology of the SARS-Coronavirus. Springer. https://doi.org/10.1007/978-3-642-03683-5_6.
Wen, K., Fang, X., Yang, J., Yao, Y., Nandakumar, K.S., Salem, M.L., Cheng, K., 2021. Recent research on flavonoids and their biomedical applications. Curr. Med. Chem. 28 (5), 1042–1066. https://doi.org/10.2174/0929867327666200713184138.
WHO, 2023 https://www.who.int/activities/tracking-SARS-CoV-2-variants/.05.07.2023.
Yan, L., Zhang, Y., Ge, J., Zheng, L., Gao, Y., Wang, T., Jia, Z., Wang, H., Huang, Y., Li, M., Wang, Q., Rao, Z., Lou, Z., 2020. Architecture of a SARS-CoV-2 mini replication and transcription complex. Nat. Commun. 11, 5874. https://doi.org/10.1038/s41467-020-19770-1.
Yin, W., Luan, X., Li, Z., Zhou, Z., Wang, Q., Gao, M., Wang, X., Zhou, F., Shi, J., You, E., Liu, M., Wang, Q., Jiang, Y., Jiang, H., Xiao, G., Zhang, L., Yu, X., Zhang, S., Eric Xu, H., 2021. Structural basis for inhibition of the SARS-CoV-2 RNA polymerase by suramin. Nat. Struct. Mol. Biol. 28 (3), 319–325. https://doi.org/10.1038/s41594-021-00570-0.
Yoon, J.J., Toots, M., Lee, S., Lee, M.E., Ludeke, B., Luczo, J.M., Ganti, K., Cox, R.M., Sticher, Z.M., Edpuganti, V., Mitchell, D.G., Lockwood, M.A., Kolykhalov, A.A., Greninger, A.L., Moore, M.L., Painter, G.R., Lowen, A.C., Tompkins, S.M., Fearns, R., Natchus, M.G., Plemper, R.K., 2018. Orally efficacious broad-spectrum ribonucleoside analog inhibitor of influenza and respiratory syncytial viruses. Antimicrob. Agents Chemother. 62 (8), e00766. https://doi.org/10.1128/AAC.00766-18. -18.
Yu, M.S., Lee, J., Lee, J.M., Kim, Y., Chin, Y.W., Jee, J.G., Keum, Y.S., Jeong, Y.J., 2012. Identification of myricetin and scutellarein as novel chemical inhibitors of the SARS coronavirus helicase, Nsp13. Bioorg. Med. Chem. Lett. 22 (12), 4049–4054. https://doi.org/10.1016/j.bmcl.2012.04.081.
Zaliani, A., Vangeel, L., Reinshagen, J., Iaconis, D., Kuzikov, M., Keminer, O., Wolf, M., Ellinger, B., Esposito, F., Corona, A., Tramontano, E., Manelfi, C., Herzog, K., Jochmans, D., De Jonghe, S., Chiu, W., Francken, T., Schepers, J., Collard, C., Abbasi, K., Claussen, C., Summa, V., Beccari, A.R., Neyts, J., Gribbon, P., Leyssen, P., 2022. Cytopathic SARS-CoV-2 screening on VERO-E6 cells in a large-scale repurposing effort. Sci. Data. https://doi.org/10.1038/s41597-022-01532-x. PMID: 35831315; PMCID: PMC9279437.
Zeng, J., Weissmann, F., Bertolin, A.P., Posse, V., Canal, B., Ulferts, R., Wu, M., Harvey, R., Hussain, S., Milligan, J.C., Roustan, C., Borg, A., McCoy, L., Drury, L.S., Kjaer, S., McCauley, J., Howell, M., Beale, R., Diffley, J., 2021. Identifying SARS-CoV-2 antiviral compounds by screening for small molecule inhibitors of Nsp13 helicase. Biochem. J. 478 (13), 2405–2423. https://doi.org/10.1042/BCJ20210201.